Ab Initio Simulations of the *K*-Edge Shift along the Aluminum Hugoniot

S. Mazevet and G. Zérah*

CEA, DPTA, Laboratoire de Structure Electronique, F91297 Arpajon, France

(Received 18 June 2008; published 9 October 2008)

We develop a first-principles approach to calculate the near-edge absorption spectrum of dense plasmas based on density functional electronic structure calculations and molecular dynamics simulations. We apply the method to the calculation of the *K*-edge shift along the aluminum shock compressed Hugoniot. We obtain a good agreement with measurements performed at moderate compression and find that the variation of the XANES spectra could be used as a signature for melting along the Hugoniot. We also show that the calculation of the *K*-edge shift along the Hugoniot formally requires a fully self-consistent calculation beyond the frozen-core approximation and provides an opportunity to test the accuracy of first principle simulation methods in the high-pressure high-temperature regime.

DOI: 10.1103/PhysRevLett.101.155001 PACS numbers: 52.50.Jm, 51.30.+i, 51.70.+f, 71.22.+i

The thermodynamical range corresponding to several times normal density and temperature of several eVs, where solids turn into dense plasmas, is of considerable interest to various fields of physics including geophysics, condensed matter, high-pressure physics, dense plasmas, and astrophysics. In this regime, the physical properties of various compounds are key ingredients in the modeling of various systems ranging from ICF capsules, the earth inner core, or the interior of Jupiter. With the recent advances of compression techniques using high power lasers or *Z* pinch, the equation of state, the electrical and optical properties of various materials ranging from the simplest systems such as hydrogen and helium to more complicated ones such as carbon, iron, or fused silica are continuously characterized both along and off the principal Hugoniot [1,2]. From the theoretical side, the use of *ab initio* electronic structure approach based on density functional theory (DFT) combined with molecular dynamics simulations and linear response theory has been rather successful at providing, to first order, a satisfying description of this complex state of matter [3]. However, the transport properties calculated have been so far limited to low frequencies (below 100 eV).

In this context, the prospect of extending the characterization of dense plasmas and shock compressed matter to near edge absorption spectroscopy is very appealing both from a theoretical and an experimental side. As realized by Bradley *et al.* [4], measurements of near edge absorption spectra of shock compressed matter brings invaluable information on the evolution of the electronic structure as the system is subject to a significant increase in both pressure and temperature. These first measurements of the *K*-shell photo-absorption edge of shocked compressed chlorine were followed by others on aluminum where a significant red shift of the edge was also observed [5,6]. From the theoretical side, several attempts have been made to combine electronic structure calculation with plasma models of varying degree of sophistication to provide a theoretical description of the near edge absorption spectra or *K*-edge photo-ionization position [7–9]. All these models suffer, however, from an inconsistency between the two treatments.

We show in this Letter that *ab initio* molecular dynamics simulations can be extended to calculate near-edge absorption spectra (XANES) of shocked compressed matter and dense plasmas. This approach provides a first-principle description of both the electronic structure and the thermodynamics state of the system by using large supercells. We apply the method to the calculation of the XANES spectra and *K*-edge shift of shock compressed aluminum which was measured experimentally.

To simulate aluminum along the principal Hugoniot, we first performed *ab initio* molecular dynamics simulations using 108 atoms initially arranged in an perfect fcc lattice.

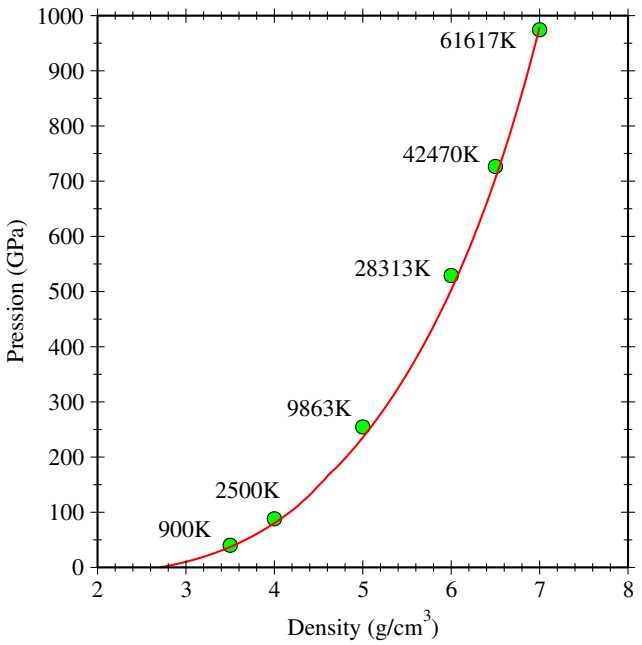

FIG. 1 (color online). Comparison between the SESAME Hugoniot and the *ab initio* calculations for Al.

The initial configuration was propagated up to 1 ps using time steps of 1 fs in the isokinetics ensemble where the velocity are rescaled at every time step to maintain the desired temperature. We used the ABINIT electronic structure code [10] and generated a PAW (Projected Augmented Wave) [11] pseudopotential in the GGA-PBE [12] parametrization of density functional theory using the *atompaw* generator [13]. The PAW pseudopotential constructed has three outer electrons ($3s^2 3p^1$) and a cutoff radius, $r_c = 1.7 a_B$. The adequacy of the pseudopotential generated is checked against all electron calculations [14].

The *ab initio* simulations were performed at the Γ point, using a plane wave cutoff of 15 Ha, and at temperatures and densities matching the SESAME principal Hugoniot [15]. The SESAME table 3700 provides a good description of aluminum at the conditions investigated here [16]. Figure 1 shows the comparison with the *ab initio* results. The agreement between the *ab initio* and SESAME pressures along the Hugoniot indicates that the PAW pseudopotential generated allows for a proper description of the aluminum thermodynamics properties and equation of state in this regime. The simulations are performed far enough from the melting point to reproduce accurately the state of the system with a liquid at 5 g/cm^3 and above and a heated fcc solid below this density [17]. Furthermore, while the cutoff chosen for the pseudopotential does not formally allow to reach the highest density, the overlap between the PAW spheres remains very moderate and does not translate in any perceptible deterioration of the thermodynamic quantities calculated at this particular condition.

To obtain the optical response in the x-ray domain along the aluminum principal Hugoniot, we select equally spaced ionic configurations along the equilibrated part of the trajectory. We then apply linear response theory as expressed within the Kubo-Greenwood formulation to the ionic configuration at hand [18,19]. This formulation leads to the real part of the optical conductivity expressed as

$$\sigma_1(\mathbf{k},\omega) = \frac{2\pi}{3\omega\Omega}\sum_{j=1}^{n_b}\sum_{i=1}^{n_b}\sum_{\alpha=1}^{3}[F(\epsilon_{i,\mathbf{k}}) - F(\epsilon_{j,\mathbf{k}})]|\langle\psi_{j,\mathbf{k}}|\nabla_\alpha|\psi_{i,\mathbf{k}}\rangle|^2\delta(\epsilon_{j,\mathbf{k}} - \epsilon_{i,\mathbf{k}} - \omega). \quad (1)$$

We employ atomic units, with the electron charge e, Planck's constant $\hbar$, and the electron mass m_e all set to unity. The i and j summations range over the n_b discrete bands (orbitals) included in the triply periodic calculation for the cubic supercell volume element Ω. The α sum is over the three spatial directions. $F(\epsilon_{i,\mathbf{k}})$ is the Fermi weight corresponding to the energy $\epsilon_{i,\mathbf{k}}$ for the ith band for the $\mathbf{k}$-point $\mathbf{k}$. The total optical conductivity is obtained by direct summation over all necessary $\mathbf{k}$-points.

Because of the use of a pseudopotential, the electrical and optical properties calculated using Eq. (1) are restricted to photon energies where the outer electrons only participate. To extend the method to the calculation of the x-ray absorption spectra, we developed the calculation of the necessary dipole matrix elements involving core electrons within the PAW (projected augmented wave) following Ref. [20]. The PAW matrix elements given by

$$\langle\psi_{m,\mathbf{k}}|\vec{\nabla}|\phi_c\rangle = \langle\tilde{\psi}_{m,\mathbf{k}}|\vec{\nabla}|\phi_c\rangle + \sum_i \langle\tilde{\psi}_{m,\mathbf{k}}|\tilde{p}_i\rangle(\langle\phi_i|\vec{\nabla}|\phi_c\rangle - \langle\tilde{\phi}_i|\vec{\nabla}|\phi_c\rangle), \quad (2)$$

reduces to

$$\langle\psi_{m,\mathbf{k}}|\vec{\nabla}|\phi_c\rangle = \sum_i \langle\tilde{\psi}_{m,\mathbf{k}}|\tilde{p}_i\rangle\langle\phi_i|\vec{\nabla}|\phi_c\rangle, \quad (3)$$

for core electrons whose wave function vanishes outside the PAW sphere of the absorbing atom. This assumes that the pseudo partial wave $|\tilde{\phi}_{\mathbf{R},n}\rangle$ form a complete basis for the pseudowave function $|\tilde{\psi}_{i,\mathbf{k}}\rangle$ within the PAW sphere. We recall that within the PAW formalism, the all-electron wave function, $|\psi_{i,\mathbf{k}}\rangle$, is connected to the pseudowave function, $|\tilde{\psi}_{i,\mathbf{k}}\rangle$, by the relation

$$|\psi_{i,\mathbf{k}}\rangle = |\tilde{\psi}_{i,\mathbf{k}}\rangle + \sum_{\mathbf{R},n}(|\phi_{\mathbf{R},n}\rangle - |\tilde{\phi}_{\mathbf{R},n}\rangle)\langle\tilde{p}_{\mathbf{R},n}|\tilde{\psi}_{i,\mathbf{k}}\rangle. \quad (4)$$

In Eq. (4), $\mathbf{R}$ represents the sphere, $\Omega_{\mathbf{R}}$, centered on each atomic site. n stands for the angular momentum l, its projection, m, and the principal quantum number, n, used when several projectors are defined. The projectors $|\tilde{p}_{\mathbf{R},n}\rangle$ vanish outside the sphere $\Omega_{\mathbf{R}}$. The partial waves $|\phi_{\mathbf{R},n}\rangle$ and the corresponding pseudo partial wave $|\tilde{\phi}_{\mathbf{R},n}\rangle$ are equal outside $\Omega_{\mathbf{R}}$. We also note that $|\phi_{\mathbf{R},n}\rangle$ form a complete basis in the spheres $\Omega_{\mathbf{R}}$.

The XANES spectrum is directly obtained using Eq. (3) in the so-called impurity model where the final state wave function, $|\psi_{m,\mathbf{k}}\rangle$, is obtained by using an excited state

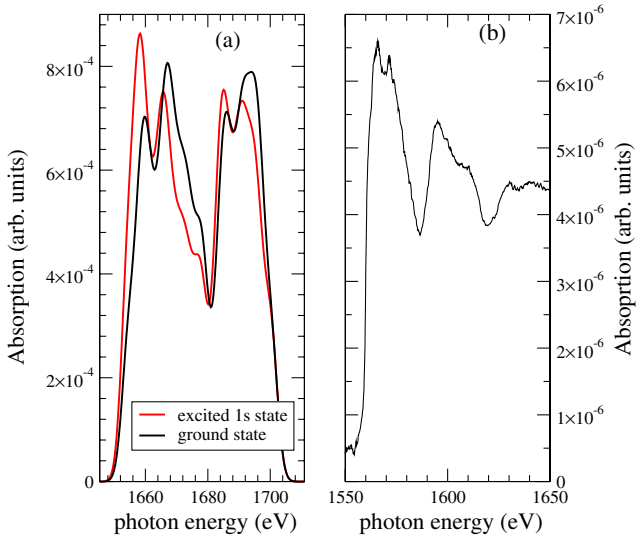

FIG. 2 (color online). (a) Calculations of the XANES spectrum at normal conditions considering the absorbing atom in a ground or excited state. (b) Experimental results [24].

pseudopotential for the absorbing atom. This pseudopotential is generated by using a hole in the 1s state of the atom while a regular pseudopotential is associated to the other atoms in the supercell. This calculation directly leads to a calculation of the final state $|\psi_{m,\mathbf{k}}\rangle$ and provides a simple way of introducing the core electron-hole interaction in the independent particle description used here [20].

Figure 2 shows the resulting x-ray spectrum for the case of aluminum and using the isolated atom 1s state wave function and energy. We compare this spectrum with a calculation using the initial state wave function where the resulting cross section is obtained by considering all the atoms in the simulation cell as absorbing ones. The resulting cross section, plotted in Fig. 2(a), is the average of these various contributions. The two calculations differ first by the position of the K-edge due to the different eigenvalues for the 1s orbitals corresponding to a ground and excited atom. This difference is, however, not significant as in either case the absolute position of the K-edge can not be obtained in the present model. This would require in addition the use of a combined GW and Bethe-Salpeter approach which is computationally to expensive to be applied to the large supercells of interest here [21].

The calculation using a hole in the 1s state of the absorbing atom provides an improved description of the first maximum in the XANES spectrum when compared to the experimental measurements shown in Fig. 2(b). However, this does not translate into the liquid state which is less structured and does not show as much difference between the two calculations. Furthermore, as we are interested here in the variation of the K-edge along the Hugoniot, we also need to consider the variation of the 1s orbital energy as both the pressure and temperature increase.

In a fully self-consistent calculation, the 1s orbital energy is affected by the change in density and temperature via the exchange correlation term in the Kohn Sham independent particle equation. This effect is referred to as a chemical shift in surface physics and is routinely used to extract informations pertaining to the local environment felt by the atom [22]. In the context of dense plasma calculations, we need to go beyond the frozen-core approximation and introduce the energy variation of the 1s orbital along the Hugoniot. In the current work, we estimate the density variation of a filled 1s orbital energy by constructing a PAW pseudopotential without a core and considering an fcc and bcc primitive cell for which the calculation can be performed. We found that this variation is independent of the crystallographic structure which suggests that it is a first order estimate appropriate for the liquid. To evaluate this variation for an excited atom in the impurity model is more ambiguous as a primitive cell is no longer representative of the system. As we are interested in the variation of the K-edge rather than the structure of the XANES spectrum, we choose to calculate the latter without considering a hole in the 1s shell of the absorbing atom as in this case, we can better quantify the variation in density of the 1s orbital energy. In addition, while the calculations using only the gamma point are well converged in the liquid phase, we found that adding k-points only slightly modifies the heights of the maxima for the solid phase. The variations observed are, however, much smaller than the ones obtained when using the absorbing atom in a ground or excited state.

Figure 3 shows the variation of the XANES spectrum calculated at the seven thermodynamical conditions mentioned previously and corrected for the variation of the 1s orbital energy. We distinguished in Figs. 3(a) and 3(b) the results corresponding to the solid and liquid phases, respectively. At 5 g/cm^3, we calculate the x-ray spectrum using snapshots from trajectories where the system was a superheated solid or in the liquid phase. Figure 3 shows that the XANES spectra preserve sharp structures in the solid phase due to the higher symmetry of the system and up to the highest density and temperature. This contrasts with the liquid phase where the spectra are far less structured at all the densities explored. This suggests that the disappearance of the maxima in the XANES spectrum may be used as a signature for melting along the Hugoniot and at high density and temperature conditions. The calculations are performed using 2000 bands which allows to converge the spectra shown to about 40 eV above the edge and also explains the sudden drop seen at large frequencies.

As we move along the Hugoniot, we see that the K-edge is gradually shifted to lower frequencies. This variation is the result of several competing effects. Figure 4(a) summarizes the variation of the various contributions. We see that the 1s orbital energy varies by about 20 eV for the density range investigated. We further point out that this calculation was performed at zero temperature and as such neglects any additional shift that could be due to temperature. The increase in Fermi energy is more moderate and is about 2 times smaller. Figure 4 also shows the variation of

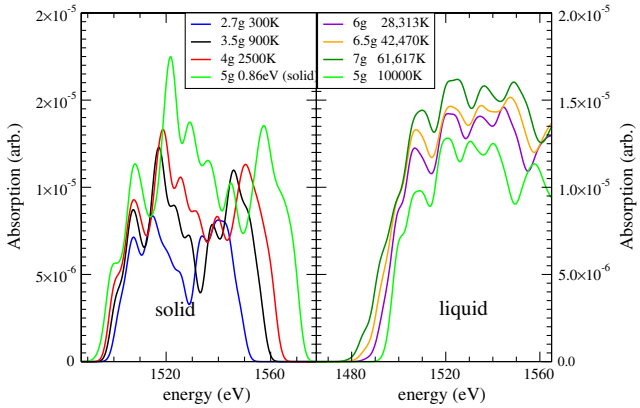

FIG. 3 (color online). (a) XANES spectra near the K-edge in the solid (a) and liquid (b) phases along the principal Al Hugoniot.

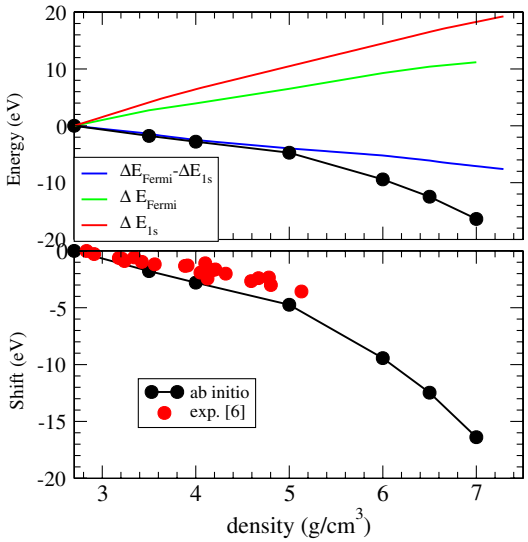

FIG. 4 (color online). (a) Individual contributions to the K-edge shift along the principal Hugoniot. (b) Comparison of the K-edge shift with the experimental measurements [6].

the K-edge position defined as a threshold value of the absorption coefficients shown in Fig. 3 ($\alpha_{\text{threshold}} = 1 \times 10^{-6}$).

For temperatures below 10 000 K, we see that the shift in the K-edge position is essentially a density effect and stays below 5 eV. We show in Fig. 4(b) a comparison with the measurements performed for aluminum [6]. We see that we have an overall good agreement with the measurements. We point out that the measurements are not performed along the principal Hugoniot. The comparison with the *ab initio* calculations along the principal Hugoniot is, however, still meaningful as the K-edge shift is only weakly dependent on temperature for these conditions. For densities above 5 g/cm^3, where the temperature along the Hugoniot rises to 5.85 eV, the K-edge shift sharply increases to reach a value of 15 eV at the highest point investigated along the Hugoniot. Here, the shift is due to the increase in temperature and the associated depopulation of the states below the Fermi energy. We also point out that the results obtained also appear to be in quantitative agreement with the prediction of previous theoretical models [5–8], and a detailed comparison will be conducted elsewhere.

An additional shift not included in the calculation could also be due to the effect of temperature on the 1s energy. Experimental measurements in this region would provide useful information on, first, the accuracy of pseudopotential calculation at high temperature and densities but also on the adequacy of the finite temperature DFT as the latter will formally bring an additional shift of the K-edge which could be accessed experimentally. Approaches have been recently proposed in the context of surface physics to relax the core orbitals self consistently [23]. This may allow us to account for both density and temperature effects on the 1s orbital energy position along the Hugoniot and needs to be investigated further in both the impurity model and in the context of dense plasmas where we use large supercells.

In summary, we developed an approach to calculate the K-edge shift and the XANES absorption spectra of dense plasmas based on first-principle electronic structure calculations and molecular dynamics simulations. The calculations reproduce the earlier measurements of the K-edge shift for moderately compressed aluminum. The calculations also indicate that the variation of the XANES spectrum could be used as a signature for melting along the Hugoniot. We also show that the calculation of the K-edge shift requires to go beyond the frozen-core approximation and provides a stringent test for the accuracy of DFT calculations at high temperatures.

The authors wish to acknowledge fruitful discussions with M. Koenig, A. Benuzzi, F. Jollet, V. Recoules, B. Siberchicot, and J. Clerouin.

*stephane.mazevet@cea.fr

[1] M. D. Knudson *et al.*, Phys. Rev. Lett. **90**, 035505 (2003); G. W. Collins *et al.*, Science **281**, 1178 (1998), and references therein.
[2] S. Brygoo *et al.*, Nature Mater. **6**, 274 (2007); J. Eggert *et al.*, Phys. Rev. Lett. **100**, 124503 (2008); D. H. Dolan *et al.*, Nature Phys. (2007).
[3] S. Mazevet *et al.*, in *Atomic Processes in Plasmas*, edited by Kilcrease, , J. S. Cohen, S. Mazevet, AIP Conf. Proc. No. 730 (AIP, New York, 2004).
[4] D. K. Bradley *et al.*, Phys. Rev. Lett. **59**, 2995 (1987).
[5] L. DaSilva *et al.*, Phys. Rev. Lett. **62**, 1623 (1989).
[6] T. A. Hall *et al.*, Europhys. Lett. (1998).
[7] F. Perrot *et al.*, Phys. Rev. Lett. **71**, 797 (1993).
[8] B. K. Godwal *et al.*, Phys. Rev. A **40**, 4521 (1989).
[9] O. Peyrusse, J. Phys. Condens. Matter **20**, 195211 (2008).
[10] X. Gonze *et al.*, Comput. Mater. Sci. **25**, 478 (2002).
[11] P. E. Blöchl, Phys. Rev. B **41**, 5414 (1990).
[12] J. P. Perdew *et al.*, Phys. Rev. Lett. **77**, 3865 (1996).
[13] N. A. W. Holzwarth *et al.*, Comput. Phys. Commun. **135**, 329 (2001).
[14] For the equilibrium volume and bulk modulus, we obtain, respectively, $V_0 = 16.98$ Å^3/atm and $K_0 = 81.59$ GPa which compare well with the all-electron calculations $V_0 = 16.48$ Å^3/atm and $K_0 = 75$ GPa.
[15] S. P. Lyon and J. D. Johnson, Los Alamos Report No. LA-UR-92-3407, 1992 (unpublished).
[16] P. M. Celliers *et al.*, J. Appl. Phys. **98**, 113529 (2005).
[17] The Hugoniot crosses the high-pressure melting line around 4.5 g/cm^3 (T_m 4700 K at $P = 132$ GPa).
[18] M. P. Desjarlais *et al.*, Phys. Rev. E **66**, 025401(2002).
[19] S. Mazevet *et al.*, Phys. Rev. E **71**, 016409 (2005).
[20] M. Taillefumier *et al.*, Phys. Rev. B **66**, 195107 (2002).
[21] G. Onida *et al.*, Rev. Mod. Phys. **74**, 601 (2002).
[22] A. Kiejna *et al.*, Phys. Rev. B **73**, 035404 (2006).
[23] M Marsman and G. Kresse, J. Chem. Phys. **125**, 104101 (2006).
[24] F. Dorchies *et al.* (private communication).